*Journal of Wind Engineering and Industrial Aerodynamics*, 20 (1985) 111—142
Elsevier Science Publishers B.V., Amsterdam — Printed in The Netherlands



# SOME COMMENTS ON THE RELATIVE MERITS OF VARIOUS WIND PROPULSION DEVICES

DR. J. F. WELLICOME

SOUTHAMPTON UNIVERSITY

ABSTRACT

This paper examines the aerodynamic characteristics of a number of devices capable of use for wind assisted fuel saving purposes. Coefficients of effective maximum forward drive force are obtained for each device based on a suitable reference area and the true wind velocity. Curves are presented for a full range of true wind course angles for each device and a number of conclusions are drawn as to the most compact wind assistance systems.

The wind assistance devices studied include the Prolss Rig, High Lift Aerofoils, Rotating Cylinders, Wind Turbines and Kites.

0304-3908/85/$03.30 

## INTRODUCTION

This paper represents an attempt to compare the characteristics of a number of wind assistance devices that could be used on merchant vessels for fuel saving purposes. The concept of "wind assistance" differs from that of total "wind propulsion" in two crucial respects : firstly the wind assistance device has to operate at higher ratios of ship's speed to wind speed and secondly there is greater pressure to produce a compact device which interferes as little as possible with the normal working of the ship.

A proper comparison of the various possible devices for wind assistance on cost benefit grounds would involve consideration of structural design, construction and maintenance costings, trading routes and operational planning, weather data, ship motions response, and so on, as well as the aerodynamic characteristics of each device. Such detailed considerations stray outside the scope of a single paper, and the comparison here will be simply on the grounds of aerodynamics, with the object of comparing the relative sizes of device needed to achieve comparable levels of fuel saving. It is, of course, appreciated that a large simple sail might make better sense than a small high lift aerofoil device of sophisticated structural design, nevertheless, a comparison of the relative sizes of these two devices for the same power saving is, of itself, of interest.

Possible wind assistance devices can be classified into two groups, one a passive group representing static devices generating lift and drag forces from airflow over the device and the other an active group which interact with normal power sources within the ship:

### Passive Devices

1) Conventional soft sail rigs
2) Soft sail improved rigs, e.g. Prolss rig
3) High lift aerofoils made from engineering materials
4) Static kites

### Active Devices

1) High lift cylinders e.g. Flettner rotors or air blown cylinder devices
2) Wind turbines either of horizontal or vertical axis types
3) Active manoeuvred kites.

In the latter group any power expended to drive the device, or power dissipated from inefficiencies in the transmission of power from the device, must be properly accounted for in assessing the net benefit from it. The basis of comparison used in this paper is an estimate of the effective net forward driving force produced by the device after making allowance for these expenditures of power. This net driving force is equivalent to a reduction in ship resistance.

Estimates of net forward driving force are expressed non-dimensionally in the form

$$C_X = \frac{R}{\frac{1}{2}\rho S V_T^2}$$

where $R$ = Effective net driving force
$S$ = Reference plan area for the device
$V_T$ = True wind speed

These esimates have been made over a range of headings to the true wind from$\Upsilon = o^{o}$ to $\Upsilon = 180^{o}$ and, as a single 'figure of merit', a simple arithmetic average of Cx over this range is quoted for each device. The use of true wind speed $V_T$ rather than apparent speed $V_A$ as the reference velocity has the advantage that at each wind angle the value of Cx is proportional to the net force acting on the ship instead of reflecting, also, changes in $V_A/V_T$ ratio with heading.

Clearly an important parameter in estimating Cx is the relation between ship speed $V_S$ and true wind speed. It has been assumed that the device is to be mounted on a cargo ship broadly comparable to an SD14 and that the ship will be operated at a constant 14 kts service speed. Wind conditions will clearly vary enormously throughout the year, but wind speeds of the order of 20 kts, or perhaps a little less, represent year round average values. Thus, the estimates quoted here have been made for a constant ratio $V_S/V_T = 0.70$

For most devices changes of $V_S/V_T$ are not critical, but wind turbines in particular perform badly at high $V_S/V_T$ ratios.

GENERAL AERODYNAMIC CONSIDERATIONS

(1) Selection of Best operating condition

Figure 1 SAIL FORWARD DRIVE COMPONENT

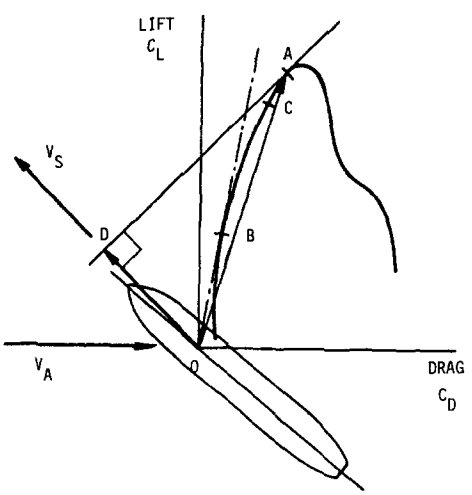


Figure 1 shows a typical rig polar diagram superimposed on a vessel to illustrate the manner of identifying the maximum forward drive force at a given apparent wind angle . Also indicated on the diagram is the operating point corresponding to the minimum aerodynamic drag angle $\varepsilon_A$(min). Point A corresponds to maximum forward drive whilst point B corresponds to minimum $\varepsilon_A$.

When matching the rig to the hull the best operating condition may be some intermediate point C between A and B. Compared to operating at point A, operating at point C, results in a significant reduction in aerodynamic side force for a small loss of drive force. There will be a consequential reduction in that component of hull hydrodynamic resistance induced by side force which compensates for the loss of rig drive force. The precise operating condition for best performance will vary with apparent wind direction, as the general level of side force varies, and it will depend on the efficiency with which the hull produces side force.

With all of the passive devices side force levels are greatest for the small apparent wind angles ($\beta$) typical of sailing close to the wind direction. With the active devices this is not necessarily so: as an example, the wind turbine generates very low levels of side force at small apparent wind angles.

However, the relatively modest sizes of rig typical of a 'wind assistance' mode rather than of a 'full wind propulsion' mode should result in relatively small levels of side force on all courses. In any case, over all courses except those close to the wind the normal optimum operating condition for a sailing vessel is close to the condition of maximum forward drive.

In order to avoid complicating the issue of comparison of rigs by considerations of matching the rig to any particular hull, the comparison made in this paper will be concerned only with operation at the maximum forward drive force condition. It is contended that in almost all situations this will correctly reflect the order of merit of each device.

(2) Theoretical limitations of High Lift Device

Clearly a compact rig requires to operate at high lift coefficient values, much higher than those encountered in normal aerodynamic practice. It is also clear from Figure 1 that the maximum forward drive condition will normally be close to the point of maximum lift coefficient for the device.

The max. obtainable $C_L$ for a two dimensional section depends on delaying the stalling process by avoiding flow separation effects associated with adverse pressure gradients on the section surface. There is an obvious incentive to design high lift aerofoils with slots and flaps designed to extend the range of $C_L$ values the section can produce.

Normal theoretical treatments of the behaviour of aerofoils of finite aspect ratio follow the Prandtl lifting line model by assuming that the trailing vortex sheet convects downstream of the foil in the direction of the onset free stream without rolling up into concentrated vortices. The same assumptions are made in lifting surface theories. Consequences of this model are that:

(i) Maximum obtainable $C_L$ values are the same as the two dimensional $C_{L\,max}$ values.

(ii) The drag induced by the vortex sheet is given by the Prandtl formula

$$C_{D_i} = \frac{k\,C_L^2}{\pi\,A}$$

for a foil of aspect ratio A. The factor k depends on planform and has a minimum value k = 1.0.

These consequences are no longer true when high $C_L$ values are employed. A correct analysis at high $C_L$ requires the direction of vortex sheet in the wake and its wrap up into a single pair of vortices to be taken into account. Appendix I gives an account of the theory of high lift devices along the lines given by Helmbold (Ref 1). Figure 3 shows that differences between the standard theory and the high lift theory are noticable at the kind of $C_L$ values typical of a conventional soft sail rig. The rig concerned is the 6 masted Dynaschiff by Prolss treated as being a simple slotted aerofoil of aspect ratio 1.2. It should be noted that including the hull as part of the foil the geometric aspect ratio of the rig plus its image in the sea surface is about 1.0. The envelope of the data for the Prolss rig, taken from Wagner Ref 2, spans a range of sail setting angles.

Two consequences stem from the high lift theory:

(i) Very high levels of induced drag can be obtained by using high values of the equivalent two dimensional $C_L$

and

(ii) Referred to the onset free stream speed and direction there is an absolute maximum coefficient for a finite aspect ratio foil given by

$$C_{L\,max} = 1.90 \times \text{Aspect Ratio}$$

corresponding to a two dimensional $C_L$ value given by

$$C_{L\,2D} = 2.6 \times \text{Aspect Ratio}$$

There is not a great body of evidence to support the Helmbold theory, but Davenport (Ref 3) quotes some jet flap data, presumably from Lowry and Vogler (Ref 4) indicating lift coefficient of the order predicted by the Helmbold theory.

## APPARENT WIND STRENGTH AND DIRECTION

Figure 2 APPARENT WIND DIAGRAM

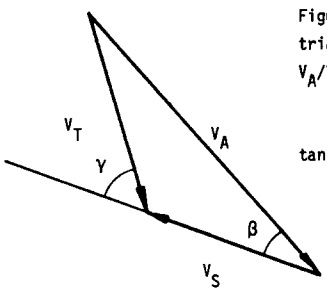


Figure 2 shows the standard apparent wind vector triangle from which the relations for $\beta$ and $V_A/V_T$ are obtained as:

$$\tan\beta = \frac{\sin\gamma}{\cos\gamma + V_S/V_T} \quad \text{and} \quad \frac{V_A}{V_T} = \frac{\sin\gamma}{\sin\beta}$$

Table 1 shows the relations between $\beta$, $\gamma$ and $V_A/V_T$ used in this paper:

| | $V_S/V_T$ = .60 | | $V_S/V_T$ = .70 | | $V_S/V_T^1$ = .542* | |
|---|---|---|---|---|---|---|
| | $\beta^\circ$ | $V_A/V_T$ | $\beta^\circ$ | $V_A/V_T$ | $\beta^\circ$ | $V_A/V_T$ |
| 0 | 0 | 1.60 | 0 | 1.70 | 0 | 1.97 |
| $20^\circ$ | 12.5 | 1.58 | 11.8 | 1.68 | 13.0 | 1.96 |
| $40^\circ$ | 25.2 | 1.51 | 23.7 | 1.60 | 26.2 | 1.88 |
| $60^\circ$ | 38.2 | 1.40 | 35.8 | 1.48 | 39.7 | 1.75 |
| $80^\circ$ | 51.9 | 1.25 | 48.4 | 1.32 | 53.9 | 1.57 |
| $100^\circ$ | 66.6 | 1.07 | 61.9 | 1.12 | 69.5 | 1.36 |
| $120^\circ$ | 83.4 | 0.87 | 77.0 | 0.89 | 87.2 | 1.12 |
| $140^\circ$ | 104.5 | 0.66 | 95.9 | 0.65 | 109.2 | 0.88 |
| $160^\circ$ | 134.8 | 0.48 | 125.0 | 0.42 | 139.3 | 0.68 |
| $180^\circ$ | 180 | 0.40 | 180.0 | 0.30 | 180.0 | 0.59 |

*$V_T^1$ refers to estimated wind strength at 100m altitude

$V_T$ refers to wind speed at 10m altitude.

The majority of the estimates of this paper use the data for $V_S/V_T$ = 0.70. The data

for $V_S/V_T$ = 0.60 was used in the wind turbine estimates and $V_S/V_T^1$ = .542 was used in the manoeuvring kite estimates.

Notice that $\beta<90^0$ for course angles up to $\gamma$ $130^0$, so that the apparent wind will be abaft the beam for only a small fraction of the time, and moreover the apparent wind will be very small when $\beta>90^0$. It is very difficult to obtain large forces on a rig in following winds unless some means is found of increasing the relative wind speed. A moving kite is the only way of achieving this result.

## PERFORMANCE OF SOFT SAIL RIGS

There is a considerable body of aerodynamic data available from wind tunnel tests on soft sail rigs, both for modern racing yachts and, through the work at Hamburg University, for a range of rigs suitable for commercial application.

FIGURE 3 PROLSS RIG - 6 MASTS
(PERFORMANCE ENVELOPE)

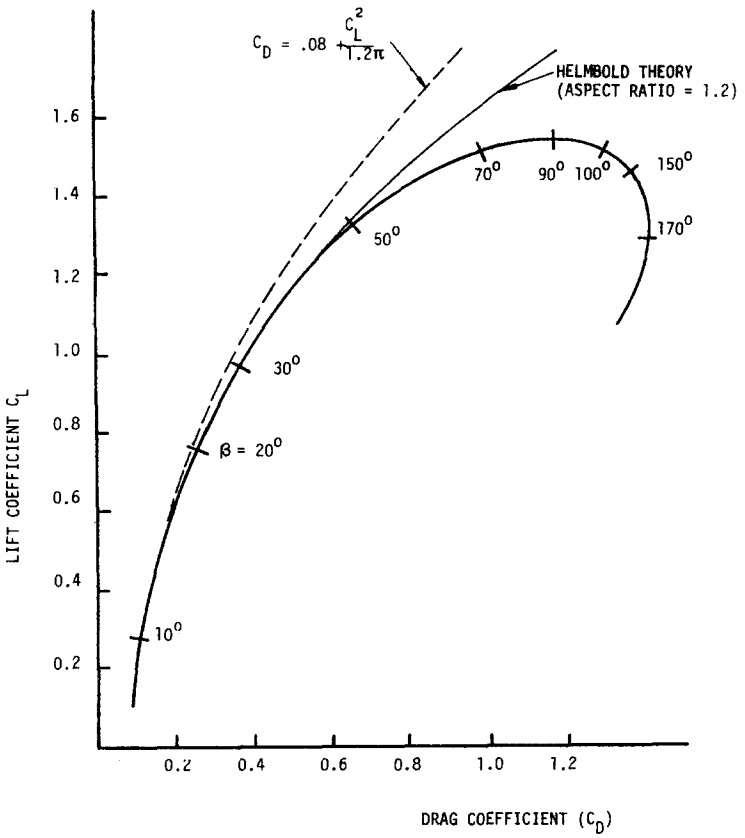


Figures 3 and 4 are drawn from data obtained by Wagner (at Hamburg) for the Prolss rig. Figure 3 is for a six-masted rig powerful enough to drive a vessel entirely by wind. The actual geometric aspect ratio of the rig, treated as a single aerofoil is quoted as 0.43. Treating the rig and the

hull together as one half of an aerofoil formed by reflecting the vessel and rig in the sea surface, and equivalent aerofoil of geometric aspect ratio 1.0 is formed. Using the wind tunnel data as a guide the envelope of all the data for various settings of the individual yard angles (mast by mast) compares well with a single foil prediction for an aspect ratio of 1.2.

FIGURE 4
PROLSS RIG - SINGLE MAST
DATA FROM WAGNER (REF 2)

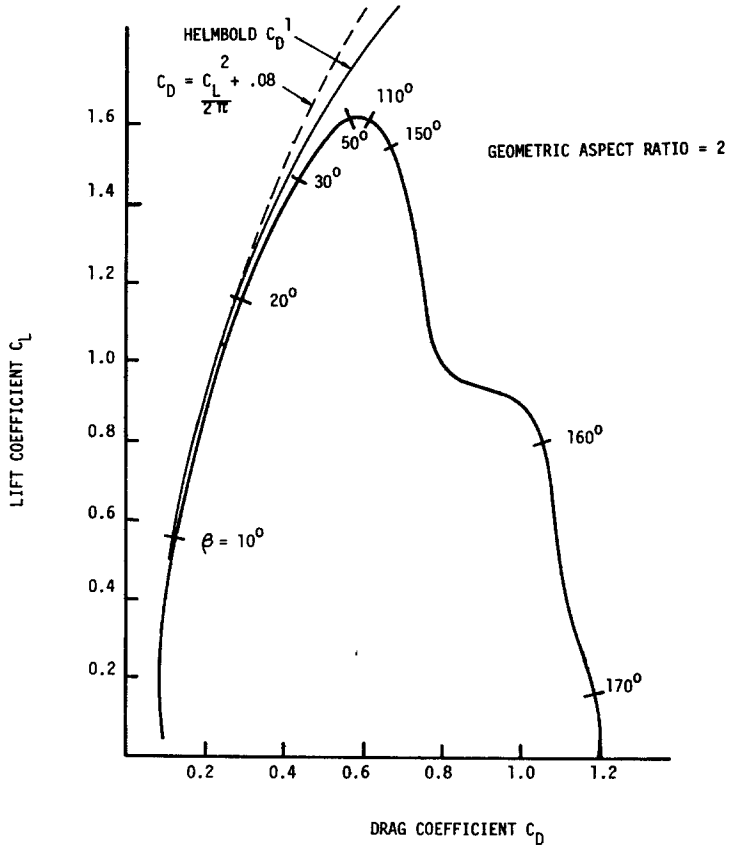


Figure 4 is for a single mast forming an aerofoil of geometric aspect ratio 2.0. In this case the nearest theoretical match is an aerofoil of aspect ratio 2.25. There is a gap between the lowest sail on the mast and the deck which is about one sixth of the mast height. The effective aspect ratio could be nearly doubled if this gap were closed, leading to a substantial reduction in $C_D$. As it is, the effective aspect ratio is about 10% greater than the geometric value due to the proximity of the deck. Curiously enough, although still present on the six masted rig, the effect of the gap between sails and deck seems to be much less significant for that arrangement.

Both Figures 3 and 4 indicate the operating point for maximum forward drive over a range of apparent wind angles . For the single mast case the rig should be operated at the maximum $C_L$ over a wide range of $\beta$ angles (from $\beta = 50^0$ to $\beta = 110^0$).

FIGURE 5 SOFT SAILS - PROLSS RIG DATA

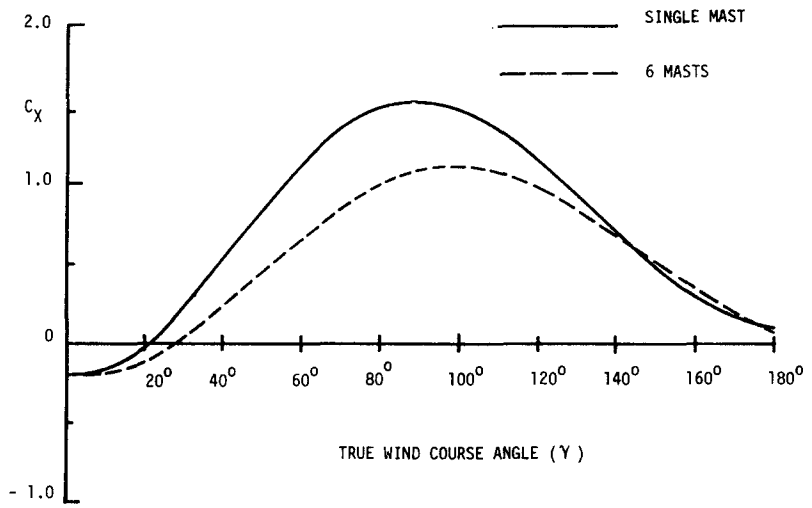


Figure 5 shows the effective drive force coefficient $C_X$ for these two rigs. Clearly the single mast is superior for all course angles up to $Y = 140^0$. This is due to the lower levels of induced drag associated with the higher aspect ratio. Closing the gap at the deck would result in a significant further improvement.

For the remainder of this paper the single mast arrangement will be used as a standard against which the other rigs are judged.

## HIGH LIFT AEROFOILS

The generation of high lift coefficients requires the control of separation round the lifting device,particularly at the trailing edge or edges, where separation will lead to a loss of circulation and the production of a thick wake leading to a high drag.

A single, thin, suitably cambered foil can be designed to reach $C_L = 1.8 \rightarrow 2.0$ and some high performance sail designs have achieved this level of performance. The addition of suitable slots and flaps can raise lift coefficients to the order $C_L = 3$. This seems to represent the limit of performance of a single foil.

In terms of compactness on board ship the diameter of cylinder enclosing the rig is perhaps a more useful parameter than the chord of the individual foils comprising a high lift aerofoil device It is possible to mount two or three foils in close proximity in a bi-plane or tri-plane arrangement without going outside a cylinder of diameter little larger than the chord of the individual aerofoils. If lift coefficient values are then computed on the basis of the projected lateral area of the device then lift coefficients of the order of $C_L = 5.0$ should be achievable, with none of the individual foils generating $C_L$ values above 2.0. On the same basis with the individual foils having profile drag coefficients of the order $0.01 \rightarrow 0.02$ an overall profile drag coefficient of the order of $C_D = 0.05$ should be achievable.

It is not part of the purpose of this paper to treat the detailed design of high lift foils. For the purpose of estimating possible benefits it would be assumed that for a two dimensional section lift and drag coefficients just before stall can reach $C_L = 5.0$ and $C_D = .05$ respectively

In order to assess the effects of rig height and aspect ratio three dimensional corrections using the Helmbold theory will be used as the $C_L$ values are well beyond the range for which the more traditional Prandtl corrections would be appropriate. There are obvious benefits in using a high aspect ratio rig, but it should be noted that the effective aspect ratio of a foil can be substantially improved by eliminating the gap between the device and the ship's deck so that the foil has effectively only one free tip to generate a trailing vortex system. This may double the effective aspect ratio of the device. Other features which can result in a significant, if less dramatic, improvement are the use of multiplane foils and the use of end plates or winglets.

FIGURE 6 LIMITING FOIL FORCES FROM HELBOLD THEORY

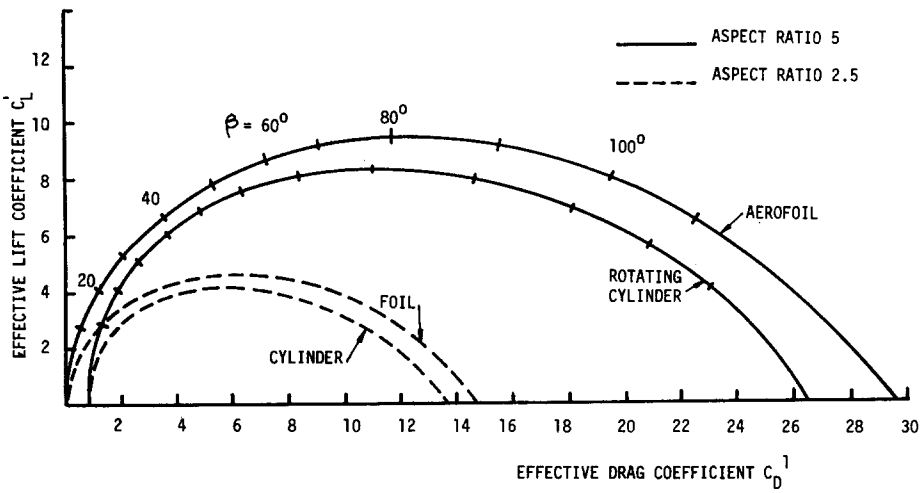


Figure 6 shows the limiting curves of $C_L^1$ vs $C_D^1$ for high lift foils according to the Helmbold theory of Appendix I. Two sets of curves are shown: for aspect ratios A = 5.0 and A = 2.5. The diagram includes curves for rotating cylinders at the same aspect ratios and indications of the maximum forward drive point at various apparent wind angles are also shown. It will be presumed that no aerofoils can operate outside these limiting curves.

FIGURE 7 HIGH LIFT AEROFOILS - MAXIMUM ATTAINABLE $C_L'$

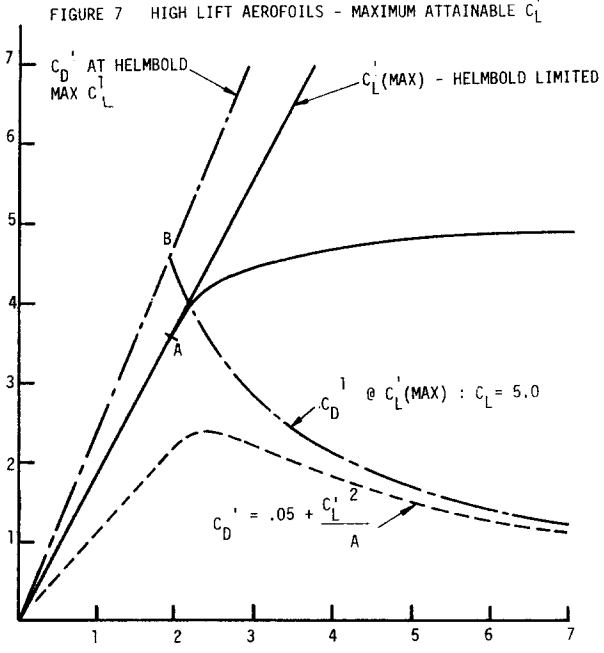


Figure 7 presents data at the max.$C_L'$ obtainable according to the Helmbold theory, both in terms of the absolute maximum obtainable and in terms of the maxima available corresponding to a two-dimensional stalling limit of $C_L$ = 5.0. Several features are of interest:-

(i) Up to the point A the value of $C_L$ at $C_L'$max is less than 5.0. This indicates that there is little point in aiming for really high $C_L$ values at aspect ratios less than two as the potential for high lift will not be usable until the apparent wind angle $\beta$ exceeds $90^0$.

(ii) Up to the point B the total drag coefficient $C_D'$ increases linearly in line with the linearly increasing usable $C_L$ value.

(iii) Beyond B total drag reduces with aspect ratio, showing considerable benefits from the use of effective ratios up to A = 5 or 6

(iv) The conventional induced drag estimate is substantially too low.

FIGURE 8 PERFORMANCE OF HIGH LIFT AEROFOILS
- PREDICTED FORWARD DRIVE COEFFICIENTS

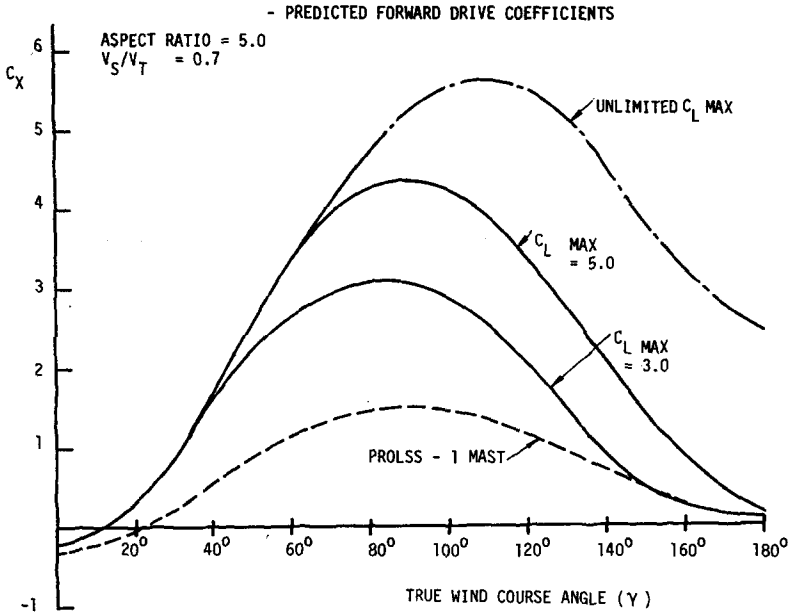


Figure 8 shows the effect of using high lift devices on the available maximum drive force coefficient $C_X$. The diagram gives three estimates for foils of aspect ratio 5. These correspond to (a) unlimited $C_L$ based on the whole of the Helmbold limit curve of Figure 6. (b) a curve assuming that the two dimensional $C_L$ is limited to 5.0 and (c) a curve assuming $C_L$ is limited to 3.0. Clearly there are substantial advantages to be gained over the single mast Proiss rig (shown dotted) over the whole range of course angles . The curve for $C_L$ max = 5.0 is probably attainable, but max $C_L$ values well beyond this level are needed to obtain significant force levels directly downwind.

## ROTATING AND BLOWN CYLINDERS

Rotating cylinders first developed by Flettner for shipboard use are one of a very small class of aerodynamic devices capable of developing really high two dimensional $C_L$ values. Thom, Ref (5), was perhaps the first to demonstrate this effect experimentally. He measured lift coefficients up to $C_L$ = 18 and his data, presented in Figure 9, shows no sign that this represents the upper limit of attainable lift. The only drawback of the device is the high drag coefficient involved compared to normal aerofoils. Thom's data was obtained at low Reynold's Numbers and the drag is evidently too high at low rotational speeds. Figure 9 shows some attempt to correct the drag below a rotational speed ratio $v/V$ = 2.0.

FIGURE 9
ROTATING CYLINDER -
TWO DIMENSIONAL LIFT AND DRAG
CHARACTERISTICS

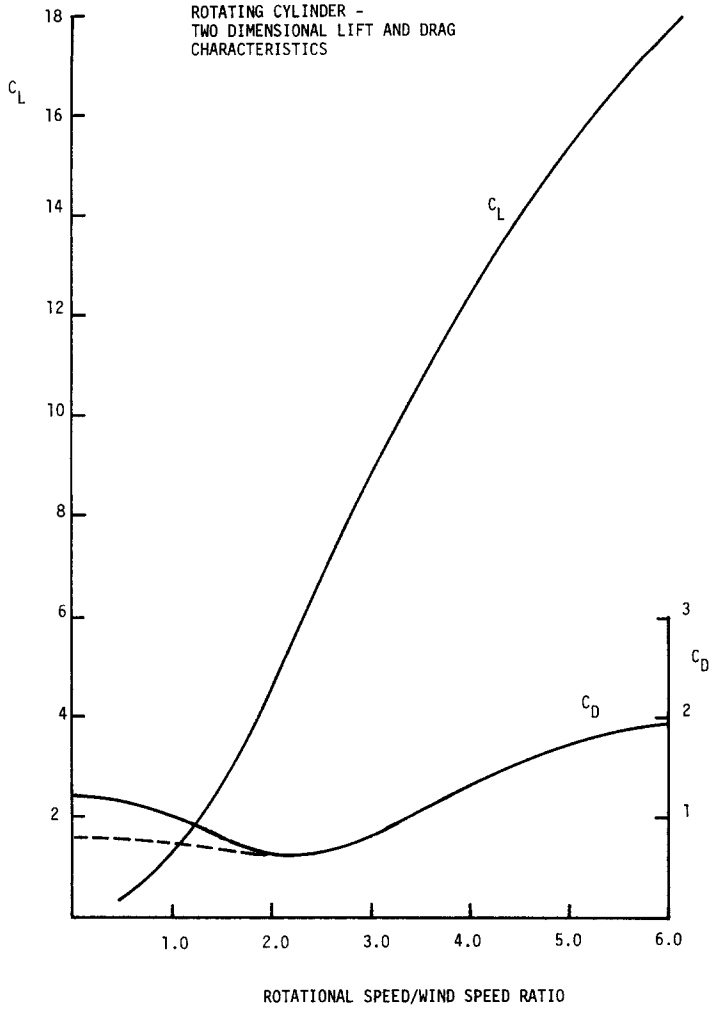

FIGURE 10

ROTATING CYLINDER - EQUIVALENT TWO DIMENSIONAL LIFT COEFFICIENTS

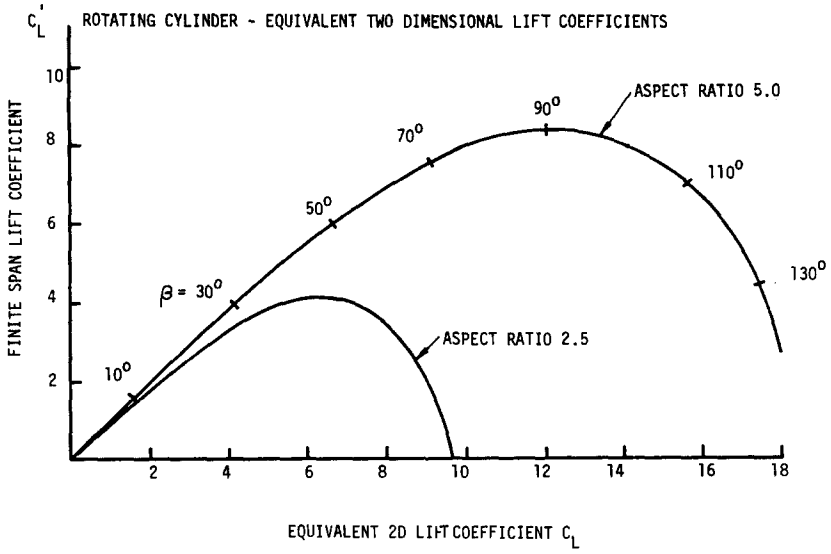


As already mentioned, Figure 6 shows $C_L^1$, $C_D^1$ curves for a rotating cylinder at aspect ratios 2.5 and 5.0. These curves have been based on the Thom data of Figure 9. Figure 10 shows the relation between the three dimensional $C_L^1$ and the equivalent two dimensional $C_L$ value for these two aspect ratio cylinders. Clearly, there is a limit to the usable $C_L$ value (which is dependant on aspect ratio). Even at aspect ratio A = 5 there is little need to go beyond $C_L$ = 12, a value that would be appropriate at apparent wind angles $\beta = 90^0$ and hence course angles $\Upsilon \approx 130^0$ to the true wind. At low $\beta$ angles quite small $C_L$ values are needed at the maximum forward drive condition.

Static cylinders which generate circulation and hence lift by air blown out through a series of slots along the cylinder surface have similar lift characteristics to the rotating cylinder and, at low levels of lift, similar drag characteristics. At high levels of lift the air used to generate lift is expelled into the wake to provide an element of jet propulsion which negates the normal drag mechanism.

In order to estimate effective forward drive force coefficients $C_X$ for this device some allowance has to be made for the power expended in rotating the cylinder or pumping the circulation control air. This has been done on the basis that, had the power concerned been supplied to the ship's propeller via the main engine the added thrust would have been equivalent to a reduction of ship resistance given by

$$\Delta R = \frac{\eta_D . P}{V_S}$$

where

$\eta_D$ = The quasi-propulsive coefficient for main propulsion

P = Power expended on generating lift

$V_S$ = Ships Speed

for calculation purposes $\eta_D$ = 0.65 was assumed.

FIGURE 11

ROTATING CYLINDER - EFFECTIVE FORWARD DRIVE FORCE

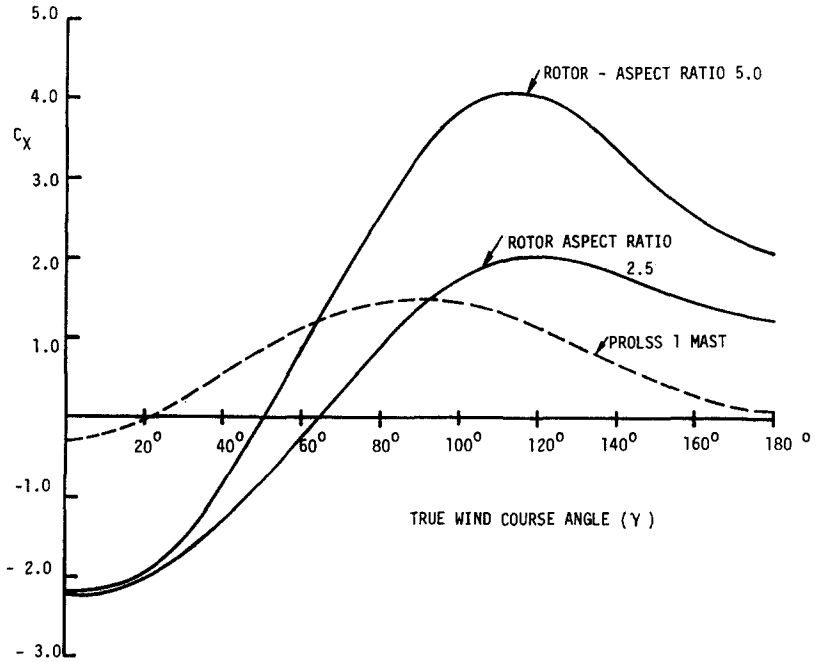


Figure 11 gives the estimated $C_X$ values for cylinders of aspect ratio 2.5 and 5.0; compared, as usual, to the single mast Prolss rig data. The following points are noteworthy:

(i) The cylinders provide substantial levels of thrust downwind, being considerably better in this respect than the high lift aerofoils.

(ii) There is a considerable drag penalty in headwinds. This is sufficient to render the net benefit of the lower aspect ratio cylinder to be marginal, and in any case might force a ship fitted with rotors to avoid sailing directly into a head wind.

## WIND TURBINES

Since the 1975 RINA Symposium on Commercial Sail there has been a steady, but low, level of interest in the use of wind turbines for ship propulsion purposes in parallel with the more serious interest in their use for power generation on land. This interest centres on the remarkable ability of the wind turbine to provide forward thrust whilst working into a headwind.

In principle there are three modes of use of a wind turbine :

(i) To extract power from the wind for transmission to the ship's propeller for propulsion purposes

(ii) To use in an autogyro mode to give direct wind propulsion

(iii) To use as an air propulsion device taking power from the main machinery.

Of these three modes only the first will be considered here, although in beam winds there may well be merits in the autogyro mode. Mode (iii) could be considered when operating downwind at speeds in excess of true wind speed.

There is an inherent difference between the use of a wind turbine for land-based power generation and for wind propulsion at sea. For power generation the object is to extract the maximum possible energy from the wind regardless of turbine drag. For wind propulsion purposes it is vitally necessary to obtain an optimum balance between energy extraction and turbine drag. As a consequence the turbine must operate at much less than the maximum level of energy extraction, particularly in headwind operation.

Assuming the windmill drag to act along the apparent wind direction and ignoring any induced drag effects due to sideforce on the hull, the net effective driving force for the wind turbine is given by

$$\Delta R = \frac{\eta_D \cdot \eta_T P}{V_S} - D \cos\beta$$

where $\eta_D$ = quasi-propulsive coefficient for the water propeller

$\eta_T$ = The power transmission efficiency between the turbine and the water propeller

$P$ = Power extracted by the wind turbine

$D$ = Aerodynamic drag of the turbine

Appendix 2 sets out an actuator disc analysis of the optimum power setting for the wind turbine This analysis was used as a basis for calcultating equivalent maximum forward drive coefficients for the wind turbine. The reference area for estimating $C_X$ for wind turbine has been taken as the turbine disc area in order to indicate the overall size of the device.

FIGURE 12

WIND TURBINE - DRIVE FORCE COEFFICIENT - VARIATION WITH $V_S/V_T$ - $\beta = 90^0$

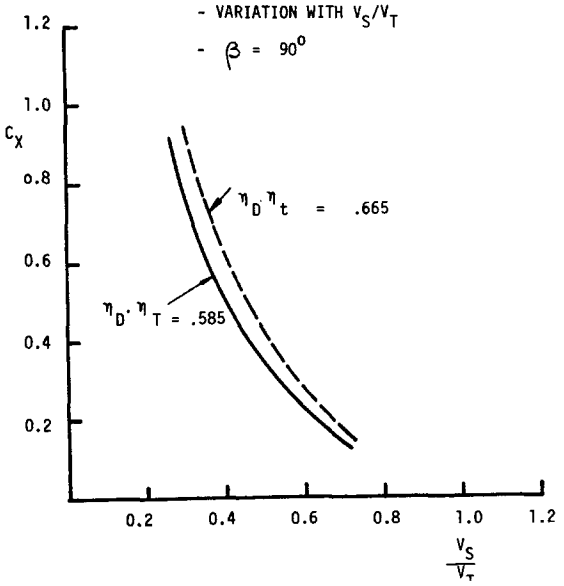

FIGURE 13
WIND TURBINE - EFFECTIVE FORWARD DRIVE FORCE COEFFICIENTS

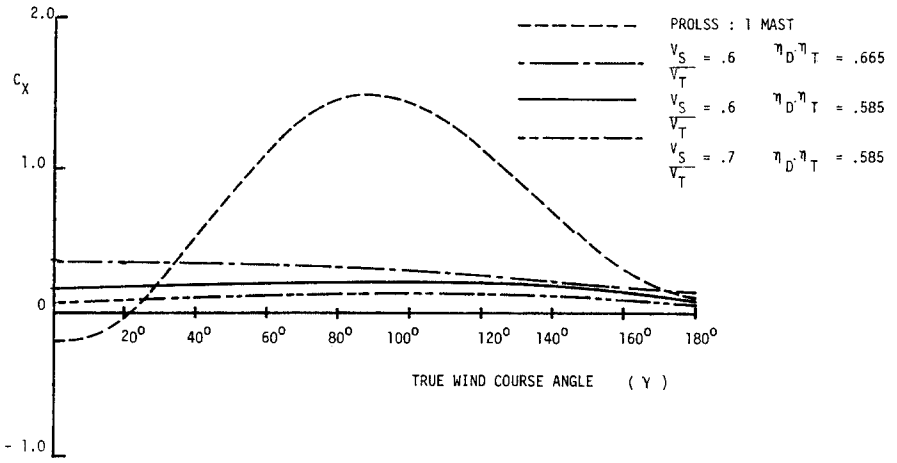


Figures 12 and 13 summarize the wind turbine performance estimates, from which the following points emerge:-

(i) Figure 12 shows how rapidly $C_X$ falls of as $V_S/V_T$ increases. At the sort of ratios typical of average wind assisted motor sailing effective driving forces are very small and any turbine device must as a consequence be very large.

(ii) Figures 12 and 13 both show how sensitive $C_X$ values are to the product of transmission efficiences and water propulsion efficiences ($\eta_T \times \eta_D$). It makes it difficult to estimate reliable performance levels for wind turbine.

(iii) Even if blade area rather than disc area is used to define $C_X$ the values achieved only compare with soft sails and are nowhere near the values achievable with other high lift devices.

(iv) The merit of the turbine is that it produces nearly uniform drive forces over the entire range of wind angles Y . In particular a net thrust is obtainable operating directly into a headwind.

KITE PROPULSION

A brief investigation has been recently carried out at Southampton University, under an SERC Contract, into the feasibility of using Kites for ship propulsion.

If propulsive forces of any consequence are to be developed using a practical Kite size it is necessary to make use of the considerable force amplification obtained by deliberately driving the Kite round the sky as a continuous process. Driving the Kite repetitively round a figure of eight manoeuvre of a suitable size at a suitable mean Kite altitude can achieve relative air speeds

five times faster than the apparent wind speed available to a static Kite. The result is that forces are of the order of 20 times greater on a moving Kite. The moving Kite can also be made to fly at a much lower altitude than its static hover altitude, resulting in a much larger fraction of the total force being available as a driving force at the ship.

Appendix 3 gives an outline of the theory developed to predict the forces generated by a manoeuvring Kite. The theory exists in three versions:

(i) A zero mass model which ignores kite and cable inertia.

(ii) A small kite mass model which uses the zero mass manoeuvre characteristics as a starting point.

and

(iii) A finite mass model as outlined in Appendix 3 which solves the equation of motion for the kite numerically without reference to the zero mass case.

Ref 6 gives versions (i) and (ii) of the theory, whilst version (iii) will be the subject of a separate report.

Methods (i) and (iii) have been used to predict the behaviour of a kite undergoing a series of figure of eight manoeuvres using estimated kite drag angles ($\varepsilon$) and cable lead angles ($\delta$) based on observations of a small recreational kite. The manoeuvres were all "horizontal" in the sense that the poles of each of the two path end circles had the same altitude.

FIGURE 14
MANOEUVRING KITE - DOWNWIND DRIVE FORCE RATIOS FOR MEAN ALTITUDE = 45°

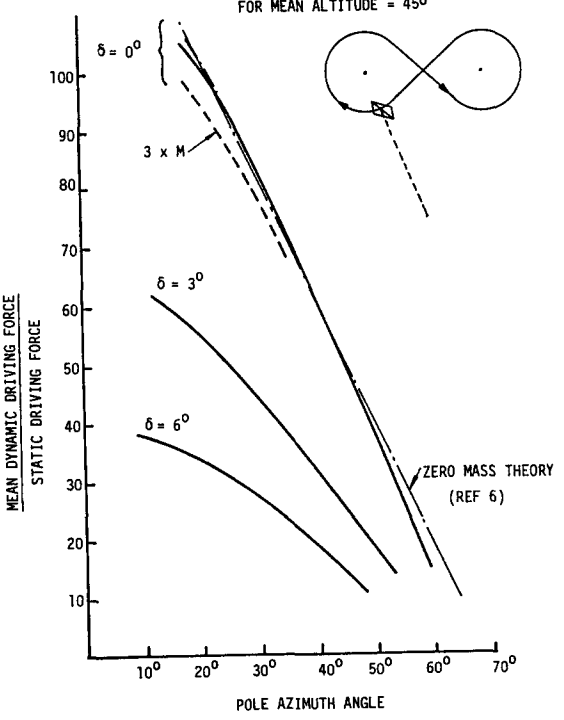

In Figure 14 the pole altitude was $45^0$, the cone angle of the closing circles $9^0$ and the azimuth angles of the poles were set equally either side of the downwind direction. The kite drag angle was taken as $8^0$. The reference force level is the horizontal component of force in the static hover condition assuming $\delta = 0^0$. The diagram shows the time averaged downwind force component at the ground end of the cable as a multiple of the reference force. The base scale is the pole azimuth angle measured from the downwind direction.

An inspection of the diagram shows that for the actual kite mass of the test kite the finite mass estimates compare very closely to the zero mass estimate taken from Ref 6 (for $\delta = 0^0$). Additional curves are shown at one third and at three times the original kite mass and it can be seen that in this case kite mass is not a significant parameter. The effect of changing cable lead angles can be seen from the curves for $\delta = 3^0$ and $\delta = 6^0$ at the standard test kite mass. This is clearly very significant. Cable lead angles will depend on cable drag and tension characteristics, but a range from about $4^0$ to $8^0$ would appear likely.

FIGURE 15

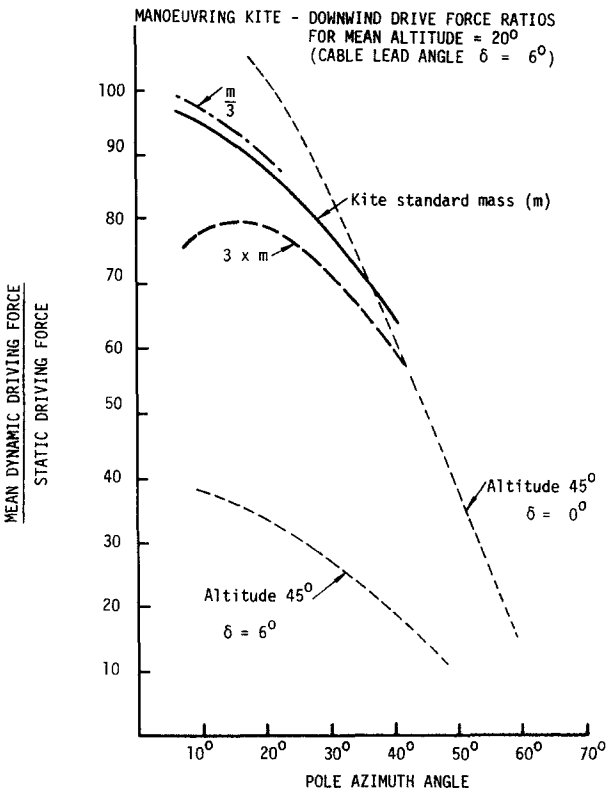


Figure 15 is a similar diagram for a kite manoeuvring round poles at $20^0$ altitude with a $5^0$ cone angle. The kite drag angle is $8^0$ and the cable lead angle is $6^0$. Again curves are drawn for the standard kite mass and for one third and three times this mass. For comparison the curves for $\delta = 0$ and $\delta = 6^0$ for the standard mass as shown in Figure 14 have also been added to the diagram.

The diagrams show conclusively that

(i) The angular position of the poles should be close together.
and
(ii) The manoeuvre should take place at low altitude.

Kites can be manoeuvred to provide a cable load at the ship at azimuth angles up to about $70^{o}$ from the downwind direction, although the flying speed will progressively fall as the kite approaches the outer limits of its potential flying arc. To assess the possible drive force available in differing directions to the apparent wind calculations were made for a plausible full scale kite using data given below:-

| Kite Data | | Manoeuvre | |
|---|---|---|---|
| Area | 200 $m^2$ | Apparent Wind Speed | 17 Kts |
| Mass | 150 kg | Azimuth Pole Separation | $30^{o}$ |
| $C_L$ | 0.65 | Pole Altitude | $20^{o}$ |
| $\varepsilon$ | $8^{o}$ | Cone Angle | $5^{o}$ |
| | $6^{o}$ | | |
| R | 300 m | | |

Figure 16 shows time average forces at the ship as a fraction of the maximum force on the kite whilst statically hovering plotted against the azimuth angle of the mean force at the ship. Figure 17 shows the times for one cycle of the manoeuvre as a function of the azimuth angle of the mean force.

FIGURE 16
MANOEUVRING KITE - FORCE AMPLIFICATION FACTORS

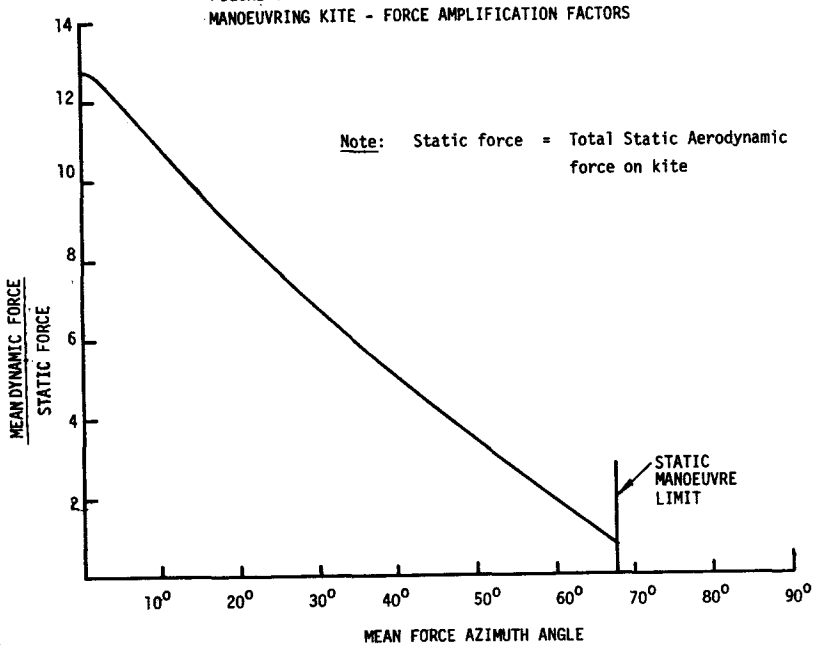

FIGURE 17
'FIGURE OF EIGHT' MANOEUVRE - TIME FOR ONE CYCLE

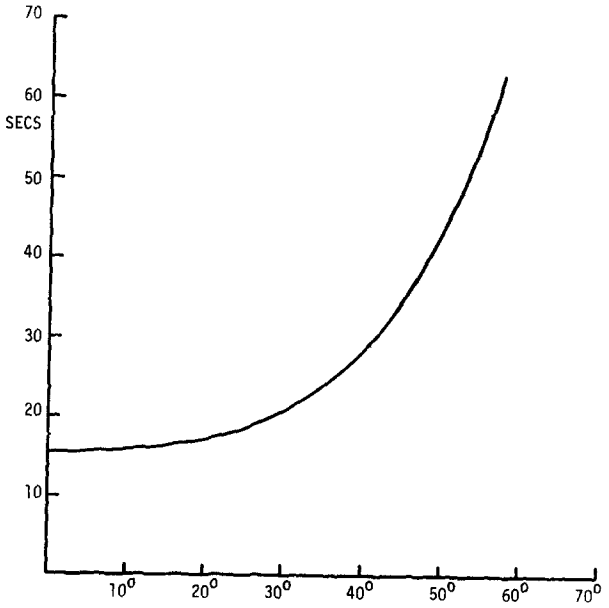


The data given in Figure 16 has been used to estimate $C_X$ data for a propulsive kite on the basis of maximum forward drive force. The calculations were made for a modest lift coefficient ($C_L = 0.65$). The zero mass kite theory indicates that flying speed is inversely proportional to sin $(\varepsilon + \delta)$. Insofar as $(\varepsilon + \delta)$ is insensitive to changes of $C_L$ it can be expected that $C_X$ will vary directly in proportion to $C_L$. This has been directly verified for the downwind case only.

In Figure 18 estimated $C_X$ values for a kite are given in comparison with the Prolss rig and also the high lift aerofoil ($C_L$ max = 5.0 from Figure 8) $C_X$ values have been based on $V_T$ at the ship using an estimate for true wind speed at an altitude of 100m

Two characteristics seem to emerge from these calculations:-

(i) Provided it is correctly manoeuvred a kite would appear to offer at least as high a drive force coefficient as any other device, including the high lift aerofoil, making it potentially the smallest device for any chosen level of wind assistance.

(ii) The kite appears capable of large drive forces directly downwind where all other devices perform badly.

FIGURE 18
KITE DRIVE FORCE COEFFICIENTS

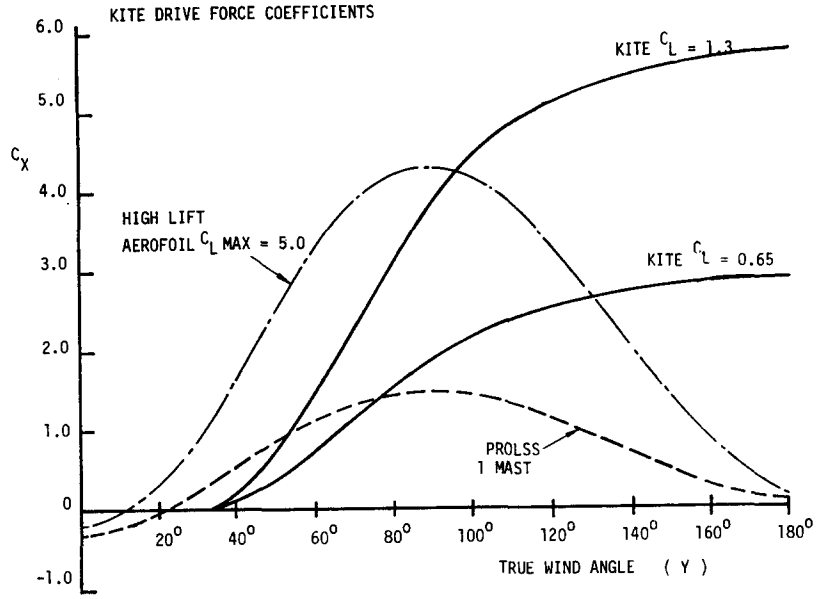


SUMMARY AND COMPARISON OF RIGS

As a single figure of merit table 2 gives mean values of $C_X$ over the whole range of wind values for each aerodynamic device considered in this paper, expressed as a multiple of the mean value for the single Prolss mast:

Table 2

| Rig | Force Factor |
|---|---|
| Prolss 1 Mast | 1.0 |
| Prolss 6 Masts | 0.72 |
| High Lift Foil : $C_L$ max = 5.0 | 3.04 |
| High Lift Foil : $C_L$ max = 3.0 | 2.09 |
| Flettner Rotor : A = 5.0 | 2.15 |
| Flettner Rotor : A = 2.5 | 0.50 |
| Wind Turbine : Middle Case | 0.30 |
| Kite : $C_L$ = 0.65 | 2.37 |
| Kite : $C_L$ = 1.3 | 4.75 |

The following comments can be made based on the above tables and the preceeding drive force coefficient estimates:

(1) On the basis of table 2 two devices stand out as potential high performance devices:

(a) the high lift aerofoil and (b) the manoeuvring kite.

(2) The wind turbine would be, by a large margin, the biggest wind assistance device for any given level of wind assistance. For a horizontal axis machine this would create problems of air draught for passing bridges in port approaches, and probably also problems in meeting stability requirements with a mill head high above the ship. For a vertical axis machine the liklihood is that its size would preclude the fitting of normal cargo handling gear.

(3) The Flettner rotor is very sensitive to aspect ratio. As a device it is hardly worth considering unless its effective aspect ratio can be made to exceed 4.0 as a rough guide.

(4) The Flettner rotor, or indeed any related device, suffers badly in head winds due to the high drag of a nearly stationery cylinder. It does, however, perform creditably downwind.

(5) The high lift aerofoil is potentially superior to all other devices at small wind angles, being captable of producing a positive forward drive force in the wind angles as low as $\gamma = 10^{o}$-$15^{o}$.

(6) The calculations suggest that a very powerful combination would be to use a high lift aerofoil for its close windedness together with a kite for its downward capability.

APPENDIX 1

HELMBOLD MODEL OF HIGH LIFT DEVICES

The Helmbold model assumes the spanwise loading on the lifting device to be elliptic with a mid span circulation $\Gamma_o$. The initial trailing vortex sheet is presumed ultimately to wrap up into a pair of concentrated vortices with the whole of the trailing vorticity lying on a plane downstream of the trailing edge at an angle $\delta$ to the onset free stream U.

The actual induced velocity over the trailing vortex sheet immediately downstream of the trailing edge is a complex affair dependant as much on the bound vortex on the lifting device as on the vortex sheet itself. The Helmbold assumption is likely to underestimate the angle at which the sheet leaves the trailing edge, rather than the reverse.

As in conventional lifting line theories the lifting device is assumed to behave like a two dimensional device operating in a local stream flow modified in direction and speed by the downwash W induced by the trailing vorticity. The downwash will be normal to the vortex sheet.

FIGURE 19 (a)

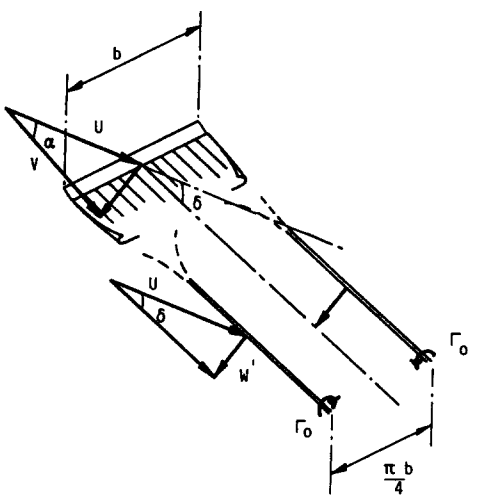


FIGURE 19 (b)

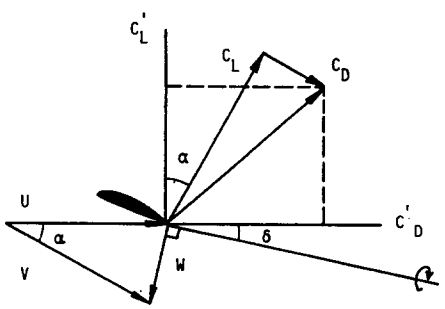


HELMBOLD MODEL OF HIGH LIFT AEROFOILS

In Figure 19 (b) $C_L$ and $C_D$ are the "two dimensional" foil properties and and $C'D$ are the "three dimensional" foil properties obtained by resolving perpendicular to and parallel to the original free stream.

Conventional calculations result in a lift and downwash at the foil due to an eliptic loading given by

$$L = \frac{\pi}{4}\rho V b \Gamma_o \qquad \text{and} \qquad W = \frac{\Gamma_o}{2b} \qquad (1)$$

These equations are presumed still to apply, a presumption which is realistic provided the wrap up process is delayed at least one span length downstream of the trailing edge.

In the far wake total vorticity is preserved by two vortices of strength $\Gamma_o$ and a horse-shoe vortex model will produce the same lift as the original eliptic loading over the span b provided the vortex separation is $\frac{\pi}{4}$ b. Helmbold justifies this far wake model on grounds of energy and momentum conservation.

The mutual induced velocity $W'$ of one trailing vortex on the other is thus given by

$$W' = \frac{\Gamma_o}{2\pi y} = \frac{2}{\pi^2} \times \frac{\Gamma_o}{b} = \frac{4}{\pi^2} \times W \qquad (2)$$

In terms of the two dimensional foil properties, the foil plan area and the local flow speed, the lift is:

$$L = \tfrac{1}{2}\rho V^2 a C_L = \frac{\pi}{4}\rho V b \Gamma_o$$

Hence
$$V.C_L = \frac{\pi}{2} \cdot \frac{b^2}{a} \cdot \frac{\Gamma_o}{b} = \frac{\pi^3}{4} \cdot A \cdot W' \qquad (3)$$

where $A = \frac{b^2}{a}$ is the foil aspect ratio

Referring forces to the free stream ahead of the foil, the effective lift coefficient is obtained from

$$L' = \tfrac{1}{2}\rho U^2 a C_L' = \tfrac{1}{2}\rho V^2 a \left[ C_L \cos\alpha - C_D \sin\alpha \right]$$

giving
$$C_L' = \left(\frac{V}{U}\right)^2 \cdot \left[ C_L \cos\alpha - C_D \sin\alpha \right] \qquad (4)$$

Similarly the effective drag coefficient is given by

$$C_D' = \left(\frac{V}{U}\right)^2 \cdot \left[ C_L \sin\alpha + C_D \cos\alpha \right] \qquad (5)$$

Figures 19 (a) and (b) can now be used to obtain the following relations between $W'$, $\frac{V}{U}$ and :-

$$W' = U \sin\delta \qquad (6)$$

$$\frac{V}{U} = \frac{\cos\delta}{\cos(\alpha - \delta)} \qquad (7)$$

$$\frac{V}{U} \times \cos\alpha = 1 - \frac{W}{U} \cdot \sin\alpha = 1 - \frac{\pi^2}{4} \cdot \sin^2\delta \qquad (8)$$
(on using (2))

$$\frac{W}{U} = \frac{\sin\alpha}{\cos(\alpha - \delta)} = \frac{\pi^2}{4} \cdot \sin\delta \qquad (9)$$

(again, on using (2))

Equation (9) can be re-written as

$$\tan\alpha = \frac{\pi^2 \sin\delta \cos\delta}{4 - \pi^2 \sin^2\delta} \qquad (10)$$

Note that in the particular case $C_D = 0$ equation (4) can be re-written as

$$C_L' = \frac{V}{U} \cos\alpha \times \frac{V}{U} C_L$$

$$= \left(1 - \frac{\pi^2}{4} \sin^2\delta\right) \times \frac{\pi^3}{4} A \sin\delta$$

or

$$C_L' = \frac{\pi^3}{4} \cdot A \cdot \sin\delta \left(1 - \frac{\pi^2}{4} \sin^2\delta\right) \qquad (11)$$

This equation is the Helmbold equation which yields a maximum value of $C_L'$ given by

$$C_L' = \frac{A}{3\sqrt{3}} \approx 1.9A$$

at $\delta = \sin^{-1}\left(\frac{2}{\sqrt{3}\pi}\right) \approx 21.6^0$

The corresponding values of $\alpha$, $\frac{V}{U}$ and $C_L$ are

$$\alpha = 51.7^0 \qquad \frac{V}{U} = 1.075 \qquad C_L = 2.6A$$

Note also that $\alpha = 90^0$ corresponds to $\delta = \sin^{-1}\left(\frac{2}{\pi}\right) = 39.5^0$

At this condition

$$C_L = 4.074A \qquad C_L' = 1.47 \; C_D \qquad C_D' = 5.98A \text{ and } \frac{V}{U} = 1.211$$

APPENDIX 2 - OPTIMUM ENERGY EXTRACTION FOR A WIND TURBINE

FIGURE 20
WIND TURBINE - ACTUATOR DISC MODEL

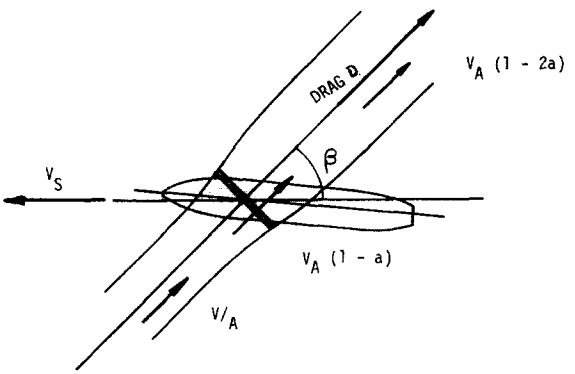


Figure 20 represents an actuator disc model of a wind turbine of disc area A. Power output and drag formulae can be defined in terms of a velocity reduction factor given, by analogy with conventional propeller theory, by the relation:

Mean Axial Flow Speed at disc = $V_1 = V_A (1 - a)$ (1)

In this equation $V_A$ is the apparent wind speed.

It will be assumed that there is an energy loss due to blade drag given by

$$\Delta E = \tfrac{1}{2} \rho A V_1^3 \cdot 4\mu = \tfrac{1}{2} \rho A V_A^3 \cdot 4 \mu (1 - a)^3 \qquad (2)$$

From this point conventional actuator disc analysis yields formulae for the power extraction from the wind (P) and turbine drag (D) of the form:-

$$P = \tfrac{1}{2} \rho A V_A^3 (1-a) \left[ 1-(1-2a)^2 - 4 \mu (1-a)^2 \right]$$

or $$P = 2\rho A V_A^3 \left[ a(1-a)^2 - \mu (1-a)^3 \right] \qquad (3)$$

and $$D = 2\rho A V_A^2 a (1-a) \qquad (4)$$

Including an allowance for hull induced resistance due to side force, the net drive force from the turbine becomes

$$\Delta R = \frac{\eta_D \eta_T P}{V_S} - D \cos \beta - K D^2 \sin^2 \beta \qquad (5)$$

The maximum net drive force is then obtained when

$$\frac{dR}{da} = \frac{\eta_D \cdot \eta_T}{V_S} \cdot \frac{dP}{da} - (\cos\beta + 2K\,D\,\sin^2\beta)\,\frac{dD}{da} = 0$$

or when $2\rho A V_A^2$

$$\left[\eta_D \cdot \eta_T \cdot \frac{V_A}{V_S}\left((1-a)(1-3a-3\mu(1-a)\right) - (\cos\beta + 2K\,D\,\sin^2\beta)(1-2a)\right] = 0$$

That is, a must be chosen so that

$$\eta_D \cdot \eta_T \frac{V_A}{V_S}(1-a)(1-3a-3\mu(1-a)) - (\cos\beta + 2K\,D\,\sin^2\beta)(1-2a) = 0 \qquad (6)$$

In this particular paper the turbine performance estimate will be on the same basis as the other rig estimates if k = o is assumed.

The case $\mu = k = o$, $\beta = 90^o$ corresponds to the point of maximum energy extraction from the wind for which a = 1/3 exactly.

The effects of blade solidity have been allowed for by carrying out a blade-element momentum calculation at one condition corresponding to $\gamma = 90^o$ for an assumed developed blade area ratio of 0.25. The results of this calculation suggests that turbine power output and drag are both about 78% of the actuator disc value and that $\mu = 0.018$. These values were assumed in subsequent calculations.

Table 3 shows the result of the optimisation calculation for a ship speed/true wind speed ratio $\frac{V_S}{V_T} = 0.60$

| Course Angle | Optimum a | Power Ratio P/Pmax | Energy Recovery $\frac{R.\,V_S}{P}$ | $C_X$ |
|---|---|---|---|---|
| 0 | .161 | .48 | .08 | .177 |
| 20 | .163 | .48 | .09 | .187 |
| 40 | .171 | .50 | .10 | .190 |
| 60 | .185 | .53 | .13 | .203 |
| 80 | .209 | .57 | .18 | .216 |
| 100 | .249 | .62 | .27 | .224 |
| 120 | .308 | .66 | .45 | .218 |
| 140 | .382 | .66 | .96 | .204 |
| 160 | .440 | .63 | 2.22 | .172 |
| 180 | .460 | .61 | 3.48 | .150 |

Note:

(1) $C_X$ coefficients are based on turbine disc area

(2) Power recovery factors become large for $\gamma > 120^o$ as turbine drag aids propulsion

(3) Pmax is the maximum power extraction for $V_A = V_T$

APPENDIX 3 - KITE MANOEUVRING THEORY

Finite Mass Model

A theoretical estimate of a moving kite has been constructed on the following basis:

(i) The kite is presumed to be manoeuvring over a spherical surface (constant radius) in a figure of eight manoeuvre comprising two great circle sweeps closed by two small circle paths between the ends of the sweep movements.

(ii) The cable drag force will be presumed to be coplanar with the kite position vector R and the kite relative wind vector V. It will be presumed to act perpendicular to R, and to be uniformly distributed along the cable length.

(iii) Cable weight will be ignored.

(iv) Cable lead angles $\delta$ and $\delta^1$ will be presumed constant through the manoeuvre and it will be presumed that $\delta = \delta^1$.

(v) Kite lift coefficient $C_L$ and drag angle $\epsilon$ will be presumed constant through the manoeuvre

FIGURE 21
KITE FORCE AND VELOCITY VECTORS

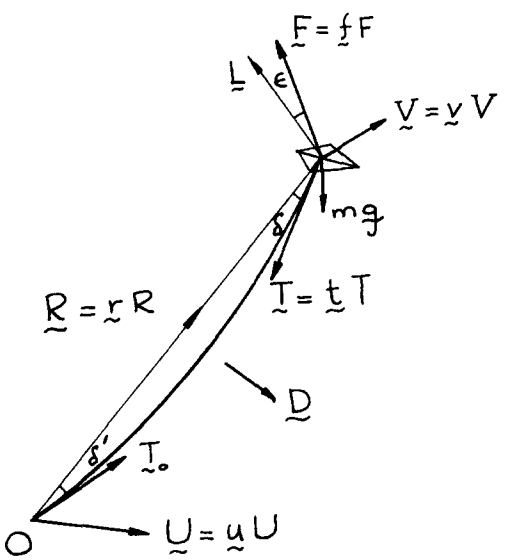

The forces acting on the kite are shown in Figure 21. The following notation has been used:-

$\underset{\sim}{U}$ = Apparent wind vector at kite as determined from ship speed and the true wind speed at the kite altitude

$\underset{\sim}{V}$ = Relative wind vector at kite determined from U and from the kite velocity R

$\underset{\sim}{F}$ = Total Aerodynamic force on the kite

$\underset{\sim}{L}$ = Lift component of F (perpendicular to V)

$\underset{\sim}{T}$ = Cable tension at Kite

$\underset{\sim}{T}_o$ = Cable tension at ship

Vectors $\underset{\sim}{u}, \underset{\sim}{v}, \underset{\sim}{f}, \underset{\sim}{t}, \underset{\sim}{r}$ are all unit vectors

FIGURE 22
CIRCULAR PATH DEFINITION

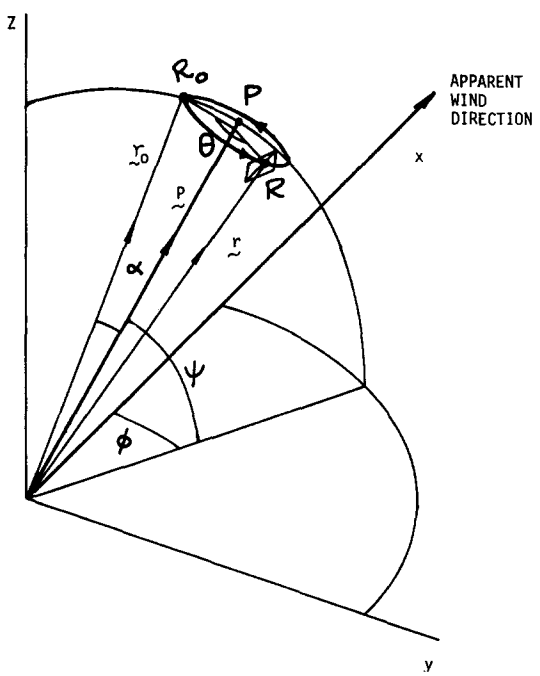

Figure 22 defines a circular path on the sphere over which the kite manoeuvres. The path takes place round a pole P (position vector $\underset{\sim}{p}R$) and the radius of the path depends on the cone angle $\alpha$, which will be constant round the path. The path is specified by the azimuth angle ($\phi$) and the altitude ($\psi$) of the pole together with the cone angle ($\alpha$).

The highest point of the path is taken as a reference point

The pole vector is $\underset{\sim}{p} = \{ \text{Cos}\phi\text{Cos}\psi,\ \text{Sin}\phi\text{Cos}\psi,\ \text{Sin}\psi \}$

The reference point $\underset{\sim}{r}_o = \{\text{Cos}\,\phi\ \text{Cos}\,(\psi+\alpha),\ \text{Sin}\,\phi\ \text{Cos}\,(\psi+\alpha),\ \text{Sin}\,(\psi+\alpha)\}$

The current kite position $\underset{\sim}{r}$, velocity $\dot{\underset{\sim}{r}}$ and acceleration are given by

$$\left.\begin{aligned} \underset{\sim}{r} &= \underset{\sim}{p}\,\text{Cos}\alpha + A(\vartheta) \\ \dot{\underset{\sim}{r}} &= \underset{\sim}{B}(\vartheta)\dot{\vartheta} \\ \ddot{\underset{\sim}{r}} &= \underset{\sim}{B}(\vartheta)\ddot{\vartheta} - A(\vartheta)\dot{\vartheta}^2 \end{aligned}\right\} \qquad (1)$$

where $\underset{\sim}{A}(\vartheta) = (\underset{\sim}{r}_o - \underset{\sim}{p}\text{Cos}\alpha)\,\text{Cos}\vartheta + \underset{\sim}{p}\times\underset{\sim}{r}_o\,\text{Sin}\vartheta$

and $\underset{\sim}{B}(\theta) = \underset{\sim}{p}\times\underset{\sim}{r}_o\,\text{Cos}\theta - (\underset{\sim}{r}_o - \underset{\sim}{p}\,\text{Cos}\alpha)\,\text{Sin}\theta$

The force balance on the kite gives an equation of motion of the form

$$m R \ddot{\underset{\sim}{r}} = T\underset{\sim}{t} + F\underset{\sim}{f} + m\underset{\sim}{g}$$

Since $\underset{\sim}{t}\times\underset{\sim}{t} = o$ and $\underset{\sim}{v}\times(\underset{\sim}{t}\times\underset{\sim}{a}) = (\underset{\sim}{v}.\underset{\sim}{a})\,\underset{\sim}{t} - (\underset{\sim}{v}.\underset{\sim}{t})\underset{\sim}{a}$

it follows after some manipulation that

$$\underset{\sim}{f} = \frac{\text{Sin}\varepsilon}{\underset{\sim}{v}.\underset{\sim}{t}}\underset{\sim}{t} + \frac{m}{F}\left\{\left(R\left(\underset{\sim}{B} - \frac{\underset{\sim}{v}.\underset{\sim}{B}\,\underset{\sim}{t})}{\underset{\sim}{v}.\underset{\sim}{t}}\right)\ddot{\vartheta} + R\left(\frac{\underset{\sim}{v}.\underset{\sim}{A}\,\underset{\sim}{t}}{\underset{\sim}{v}.\underset{\sim}{t}} - \underset{\sim}{A}\right)\dot{\vartheta}^2 + \frac{\underset{\sim}{v}.\underset{\sim}{g}}{\underset{\sim}{v}.\underset{\sim}{t}}\underset{\sim}{t} - \underset{\sim}{g}\right\} \qquad (2)$$

This can be written as

$$\underset{\sim}{f} = \underset{\sim}{a} + \underset{\sim}{b}\ddot{\vartheta}$$

where a and b are functions of $\vartheta$ and $\dot{\vartheta}$

$\underset{\sim}{f}$ is a unit vector, so that on taking the scalar product a quadratic equation for $\ddot{\vartheta}$ is formed

$$\underset{\sim}{b}.\underset{\sim}{b}\ddot{\vartheta}^2 + 2\,\underset{\sim}{a}.\underset{\sim}{b}\ddot{\vartheta} + \underset{\sim}{a}.\underset{\sim}{a} = 1.0$$

The root corresponding to positive cable tension is the only admissable root.

In effect, at each point on the arc we can determine $\ddot{\vartheta}$ from an equation of the form

$$\ddot{\vartheta} = H(\vartheta, \dot{\vartheta})$$

For the present calculation this equation has been solved numerically using a finite difference method and a constant time step through the manoeuvre.

Zero Mass Model

Putting kite mass m = o into equation (2) leads to the result

$$\underset{\sim}{t} = -\underset{\sim}{f} \text{ and } \frac{\text{Sin } \epsilon}{\underset{\sim}{v}.\underset{\sim}{t}} = -1$$

Geometric considerations lead to the relation

$$\underset{\sim}{t} \text{ Sin}\beta = \underset{\sim}{v} \text{ Sin}\delta - \text{Sin } (\beta - \delta)$$

where $\underset{\sim}{v}.\underset{\sim}{r} = \text{Cos}\beta$

It follows that in the zero mass case $\beta = \frac{\pi}{2} - (\epsilon + \delta)$

The relative velocity at the kite is given by

$$V\underset{\sim}{v} = U\underset{\sim}{u} - \underset{\sim}{B}R\dot{\vartheta}$$

so that $V\,\underset{\sim}{v}.\underset{\sim}{r} = U\,\underset{\sim}{u}.\underset{\sim}{r}$ Since $\underset{\sim}{r}.\underset{\sim}{B} = o$

Thus $\frac{V}{U} = \frac{\underset{\sim}{u}.\underset{\sim}{r}}{\underset{\sim}{v}.\underset{\sim}{r}} = \frac{\underset{\sim}{u}.\underset{\sim}{r}}{\text{Sin } (\epsilon + \delta)}$

and also $\left(\frac{V}{U}\right)^2 = 1 - 2\,\underset{\sim}{u}.\underset{\sim}{B}\,\frac{(R\dot{\vartheta})}{U} + \underset{\sim}{B}.\underset{\sim}{B}\left(\frac{R\dot{\vartheta}}{U}\right)^2$ (3)

Thus, in the zero mass case the angular velocity $\dot{\vartheta}$ can be determined directly as a function of angular position $\vartheta$ .

REFERENCES

(1) HELMBOLD H.B. Limitations of Circulation Lift
JOURNAL OF THE AERONAUTICAL SCIENCES Vol 24 No.5
March 1957

(2) WAGNER B Sailing Ship Research at the Hamburg University
SYMP ON THE TECHNICAL & ECONOMICAL FEASIBILITY
OF COMMERCIAL SAILING SHIPS
LIVERPOOL POLYTECHNIC February 1976

(3) DAVENPORT F.J. A Further Discussion of the Limiting Circulatory
Lift of a Finite Span Wing
JOUR. AERO. SCIENCES December 1960

(4) LOWRY J. G. & VOGLER R.D Wind Tunnel Investigations to Determine the effect
of Aspect Ratio and End Plates on the Rectangular
Wing with Jet Flaps Deflected $85^{o}$
NACA TN 3863 December 1956

(5) THOM A Effect of Discs on the Air Forces on a Rotating Cylinder
AERO RES. COMMITTEE R & M No. 1623 1934

(6) WELLICOME J.F. & WILKINSON S Ship Propulsive Kites - An Initial Study
Ship Science Department Report SSSU 19
December 1984